The Role of Intercalated Water in Multilayered Graphene Oxide

Muge Acik,[†] Cecilia Mattevi,[‡] Cheng Gong,[†] Geunsik Lee,[†] Kyeongjae Cho,[†] Manish Chhowalla,[‡] and Yves J. Chabal[†,§,*]

[†]Department of Materials Science and Engineering, University of Texas at Dallas, Richardson, Texas 75080, United States, and [‡]Rutgers University, Materials Science and Engineering, Piscataway, New Jersey 08854, United States. [§]Present address: Department of Materials, Imperial College, London, U.K. SW7 2AZ.

ABSTRACT A detailed *in situ* infrared spectroscopy analysis of single layer and multilayered graphene oxide (GO) thin films reveals that the normalized infrared absorption in the carbonyl region is substantially higher in multilayered GO upon mild annealing. These results highlight the fact that the reduction chemistry of multilayered GO is dramatically different from the single layer GO due to the presence of water molecules confined in the ~1 nm spacing between sheets. IR spectroscopy, XPS analysis, and DFT calculations all confirm that the water molecules play a significant role interacting with basal plane etch holes through passivation, *via* evolution of CO_2 leading to the formation of ketone and ester carbonyl groups. Displacement of water from intersheet spacing with alcohol significantly changes the chemistry of carbonyl formation with temperature.

KEYWORDS: graphene oxide · water chemistry · ketones · infrared spectroscopy · intercalation

Graphene oxide (GO) has been considered for a number of applications involving tunable optoelectronic properties through reduction in the form of thin films[1] or as a bulk powder material[2] for high capacity chemical storage applications.[3] Graphite oxide is synthesized by strong acid/base treatments[4−6] of graphite resulting in the incorporation of oxygen in many forms, such as out of plane epoxide and hydroxyl species, edge functionalization (carboxyls, carbonyls, hydroxyls) and in-plane structures (ether-like species),[7] and can be further exfoliated into separate GO sheets.[8−10] GO is a nonstoichiometric,[11] highly hygroscopic[34] compound that is electrically insulating. The key to some electronic applications with graphene oxide is therefore efficient reduction toward graphene.

Theoretical and experimental studies have focused on understanding the structure and chemistry of single layer GO, both in as-synthesized[12] and reduced forms[13] as well as the evolution of structure at different degrees of reduction.[14,15] Thermal reduction of GO for instance has been shown to involve the removal of epoxide and hydroxyl groups by formation of H_2O, H_2, O_2 (oxygen elimination), and also CO and CO_2 (carbon elimination) thus creating defects in the form of etch holes within the graphene basal plane.[16,17] There is however little understanding of the behavior of multiple GO sheets that are stacked together in the form of thin films or as bulk materials for various energy applications.[18] The interactions along the *c*-axis perpendicular to the GO sheets in the multilayered material have been mostly ignored. The multilayered structure assembled from exfoliated GO sheets is different from that of graphite oxide in that there is little or no commensurate stacking among the layers.[19] Thus interactions among layers in multilayered GO are not strictly defined by the $\pi-\pi$ interactions as in graphite but are dominated by hydrogen bonding of functional groups and trapped molecules between the layers.[20]

More specifically, reference to the presence of water and to strong interactions between GO planes has been made,[21] but little is known about the nature and role of water trapped within the ~1 nm[22,23] spacing between the sheets at the interface, and the chemistry it can foster especially during the reduction process. Yet, control of 3D multilayered GO structures is important for a number of applications, including electrolytes within supercapacitors and hybrid capacitors[24] and batteries (ionic transport),[25] mechanical actuators[26] that convert external stimuli such as thermal, light, electrical,[27,28] or chemical energy to mechanical energy.[29] For instance, in electromechanical resonators, the actuation depends on the variation of humidity and/or temperature.[30] In supercapacitors, the ion transport is controlled by the size of openings (*i.e.*, holes in GO layers) as well as the

*Address correspondence to chabal@utdallas.edu.

Received for review July 30, 2010 and accepted September 24, 2010.

Published online Xxxxxxxxx 00, 0000
10.1021/nn101844t

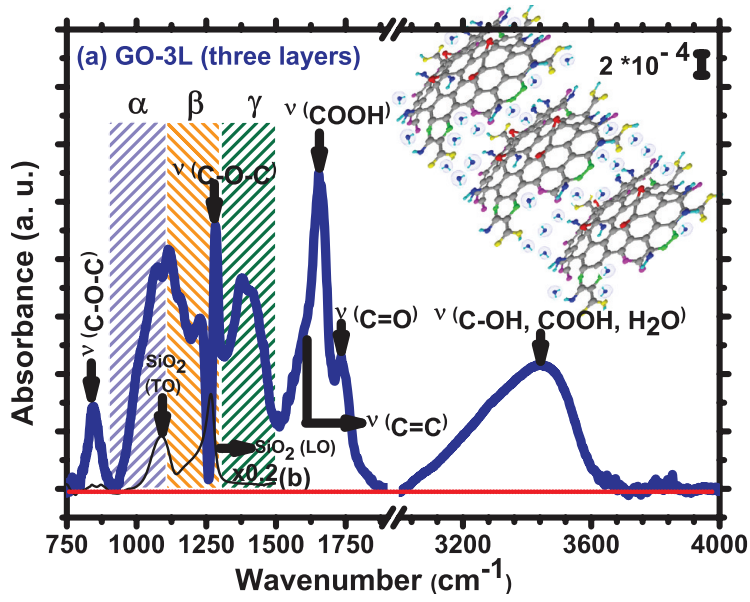

Figure 1. Infrared absorbance spectrum of GO (three layers) at room temperature. (a) Vibrational modes are shown for hydroxyls (possible COOH and H_2O) (C−OH, 3000−3700 cm^{-1}), carbonyls (C═O, 1750−1850 cm^{-1}), carboxyls (COOH and/or H_2O) (1650−1750 cm^{-1}), sp^2-hybridized C═C (in-plane stretching, 1500−1600 cm^{-1}), epoxides (C−O−C, 1280−1320 and 800−900 cm^{-1}), and some overlapped regions such as α-region (lactols, peroxides, dioxolanes, hydroxyls, 1,3-dioxan-2-ones, anhydrides, carboxyls, epoxides, 900−1100 cm^{-1}), β-region (oxolan-2-ones, peroxides, ethers, ketones, pyran-2,3-diones, lactols, anhydrides, epoxides, *o*-benzoquinones, *p*-benzoquinones, 1100−1280 cm^{-1}), and γ-region (ethers, epoxides, peroxides, ketones, *m*-benzoquinones, *p*-benzoquinones, 1280−1500 cm^{-1}) within blue, orange, and green dashed lines, respectively. Absorbance unit is abbreviated as "a.u." Each species is identified with certain colors: epoxides (red), ethers (green), COOH (yellow), C═C (gray), C═O (pink), H for H_2O (aqua), and O for H_2O (blue), using the ACD/ChemSketch Freeware, version 10.00, Advanced Chemistry Development, Inc., Toronto, ON, Canada, www.acdlabs.com, 2006. (b) Vibrational modes of SiO_2 (TO and LO) appear at ∼1078 and 1240 cm^{-1}, respectively.

intersheet spacing.[31] Mechanical properties of GO paper-like composites are controlled by network of hydrogen bonds, the concentration of which can vary with water content.[32] It is therefore of fundamental importance to understand the chemistry of water confined between the sheets in pristine GO as well as reduced GO.

We present here a detailed spectroscopic study of the chemical evolution of GO upon thermal reduction, with a quantitative comparison of interactions in *single*- and *multi*-layer GO. Direct evidence is presented for the role of water trapped between adjacent GO layers in enhancing the formation of hydroxyl and carbonyl species. Reorganization of water network or replacement of water by alcohol in the intersheet space can lead to different thermally activated chemistry, supporting the role of trapped water. Our work provides insight into how the chemical reactions can be tailored by introducing liquids between the GO sheets, which could potentially open up new pathways for studying chemical reactions in nanoscale confined space.

Infrared absorbance spectra of typical multilayered GO (three-layer and multilayers) thin films in transmission are shown in Figure 1 and Supporting Information, Figure S1, respectively. Several distinct vibrational modes of various types of oxygen functionalities can be readily identified, namely, epoxides (C−O−C, 1280−1320 and ∼850 cm^{-1}), edge carboxyl groups (COOH, 1650−1750 cm^{-1} with C−OH modes at *ca.* 3000−3700 cm^{-1}), carbonyls (C═O and O−C═O, 1750−1850 and 1500−1750 cm^{-1}, respectively), basal plane hydroxyls and phenols (edge hydroxyls)[33] (C−OH, 3000−3700 cm^{-1}), and asymmetric vibrational stretching of sp^2-hybridized C═C (1500−1600 cm^{-1}). These oxygen functionalities are common to all multilayered and single-layer GO films (Supporting Information, Figure S2) although the absolute intensities scale with the amount of material on the substrate. More specifically, various ketone and ester carbonyls are initially present as summarized in Supporting Information Table S1. With support from theoretical calculations, it is established that these chemical species have spectral contributions consisting of bending and stretching vibrational modes that overlap in α, β, and γ regions highlighted in Figure 1.

The presence of *physisorbed* water[34] is observed on single layer GO (GO-1 L) surfaces, as evidenced by both OH stretching (*ca.* 3000−3500 cm^{-1}) and scissor (1600−1650 cm^{-1}) modes of H_2O that are broadened through hydrogen interactions with C−OH (O−H stretch at 3000−3700 cm^{-1}) and COOH (OH stretch at ∼3549 cm^{-1}). These modes are markedly stronger and broader in multilayered GO (GO-ML) due to trapped water in interlayer nanospacings,[35] as a result of a high hydroxyl concentration as well as stronger hydrogen bonding interactions between OH and other oxygen functionalities in close proximity.

The presence of water dramatically influences the chemistry of multilayered GO upon mild heating (60−250 °C). This is highlighted by plotting the differential spectra in Figure 2 (*ca.* 1100−1850 cm^{-1} spectral region) for single layer GO (Figure 2i) and three-layer GO (Figure 2ii). Although the initial spectra are similar, the *relative* increase in intensity of the β and γ regions is much higher for three-layered or multilayered GO (Figure 2ii-d,e and Supporting Information Figure S3d−f, respectively) as the sample is annealed to 175 °C. Importantly, this intensity increase takes place at lower temperatures in multilayered GO (∼125 °C) than for GO-1 L

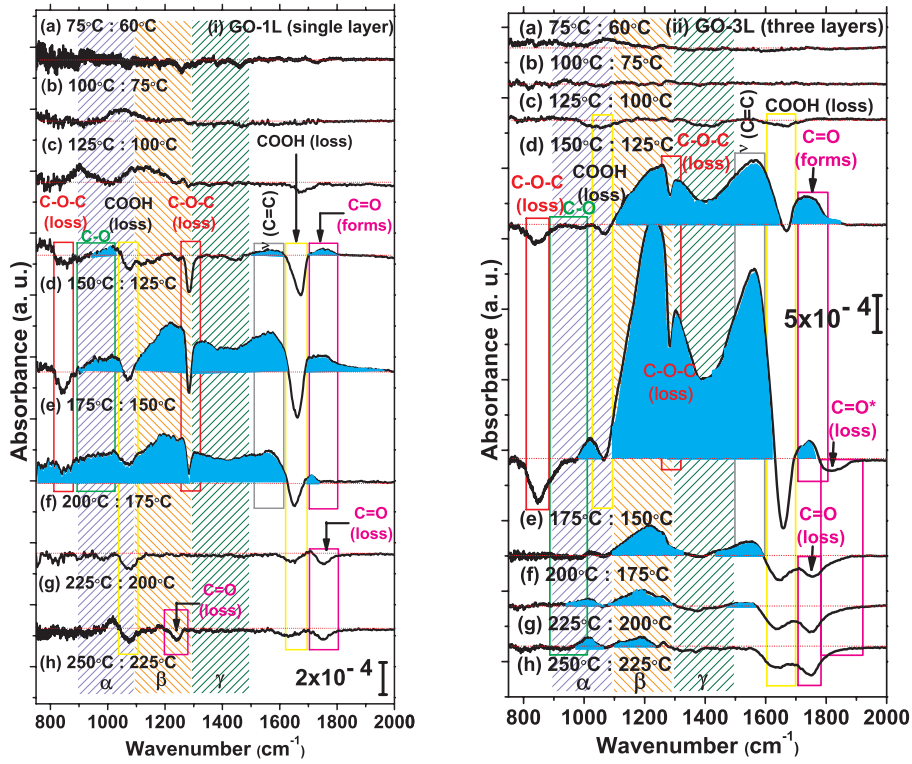

Figure 2. Comparison of infrared differential spectra of (i) single layer and (ii) three layers of GO in the 60−250 °C range. Absorbance change in functional groups are shown within temperatures of (a) 60−75 °C, (b) 75−100 °C, (c) 100−125 °C, (d) 125−150 °C, (e) 150−175 °C, (f) 175−200 °C, (g) 200−225 °C, and (h) 225−250 °C. Loss of epoxides and carboxyls are shown within red and yellow solid lines while formation/loss of carbonyls are in pink solid lines and formation of ethers in green and C═C in gray. Absorbance unit is abbreviated as a.u. Frequency regions such as α-, β-, and γ- are highlighted with blue, orange, and green dashed lines, respectively. Infrared enhancement is shown with aqua regions.

(∼150 °C). These observations indicate that, for a given number of oxygen functionalities, a larger relative concentration of ketone and ester carbonyl derivatives (*ca.* 1500−1850 cm^{-1}) is produced in GO-ML than on GO-1 L. Correlated with these observations is an intensity loss of OH related vibrational modes.

Figure 3 quantifies the findings described above by showing the dependence of the integrated intensities of the H_2O and OH (C−OH, COOH) stretching modes (*ca.* 3000−3700 cm^{-1}) in Figure 3i and the normalized concentration of carbonyls (1100−1850 cm^{-1}) as a function of annealing temperatures in Figure 3ii. Figure 3i highlights the fact that a substantial amount of water is trapped between layers of multilayered GO and that there is a precipitous drop in water concentration at ∼150 °C. In contrast, single layer GO is characterized by OH stretch region primarily arising from carboxyls and hydroxyls with relatively insignificant contribution from physisorbed H_2O. Consequently, there is no sharp loss of OH stretch intensity at ∼150 °C in GO-1 L.

In Figure 3ii, the integrated area associated with carbonyl formation is normalized to the total area of all oxygen functionalities prior to annealing. While there are marked variations in dipole moments, using this overall integrated area provides an excellent *average* measure of the total number of oxygen present in the sample and avoids uncertainties related to the degrees of surface coverage. The results clearly show that (1) the formation of carbonyls starts at lower temperatures (∼125 °C) in three-layered or multilayered GO than in single layer GO (∼150 °C), and (2) the amount of carbonyl formed is ∼4 times larger, for an identical initial oxygen concentration (in all the functional forms), for GO-3 L than for GO-1 L (∼110% increase instead of ∼30% shown in Figure 3ii). A further proof for a larger carbonyl formation during annealing of multilayered GO is provided by XPS measurements. The deconvolution of the O 1s peak (Supporting Information, Figure S4a) at *ca.* 25−350 °C in multilayered GO shows an increase of C═O component along with a loss of C−O at 150−200 °C, which are larger than for GO-1 L (Supporting Information, Figure S4b). The effect of the presence of carbonyl groups on the total carbon to oxygen ratio in multilayered GO with respect to GO-1 L can be seen in Supporting Information, Figure S5. Taking into account the extra carbonyl groups, the carbon-to-oxygen ratio is calculated with (Supporting Information Figure S5a) and without (Supporting Information Figure S5b) C═O component as a function of annealing temperatures.

The role of confined water in altering the chemistry of multilayered GO upon mild annealing can be further elucidated by understanding the mechanisms of carbonyl formation at ∼125 °C, which is accompanied by the evolution of CO_2 (Supporting Information Figure

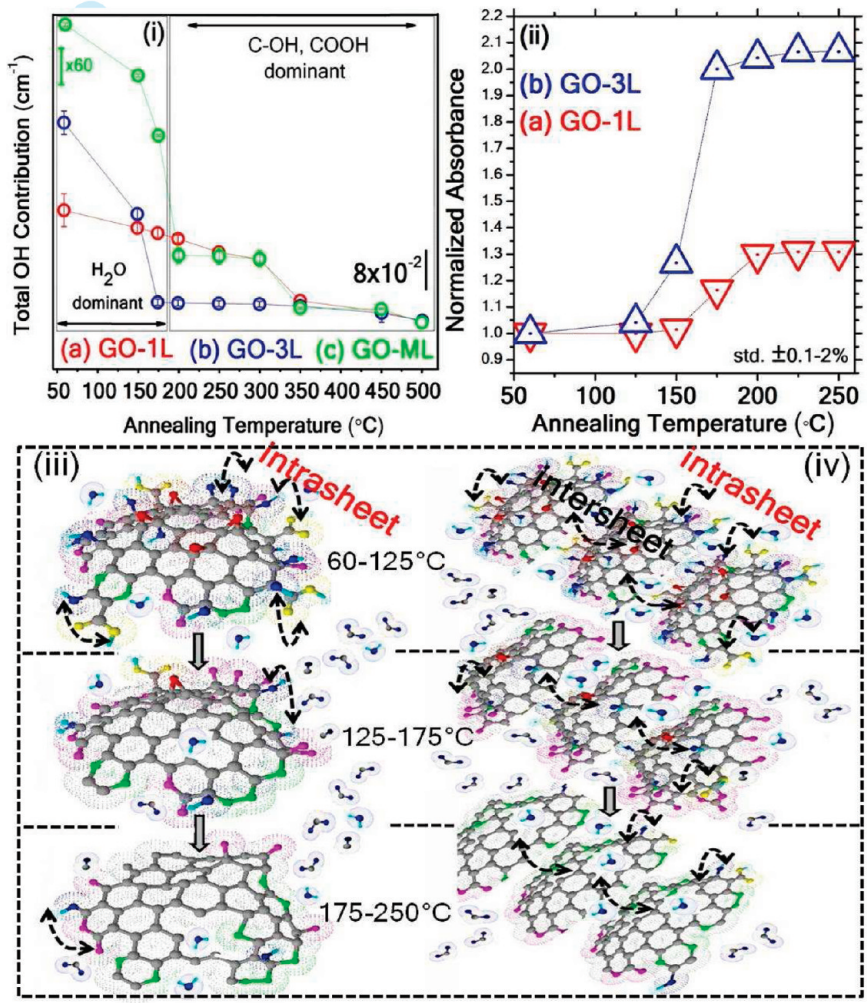

Figure 3. Comparison of the integrated total OH contribution from H_2O, OH, and COOH and normalized absorbance of integrated carbonyl concentration. (i) Integrated intensities (3000−3700 cm^{-1}, std. ± 0.01−0.2%) of C−OH peak are shown as a function of temperature for GO-1 L (red), GO-3 L (blue), and GO-ML (green). Removal of H_2O up to 175 °C significantly decreases the intensity of the C−OH peak (left). After removal of H_2O, the intensities of C−OH and COOH groups are dominant (right). (ii) Comparison of the normalized integrated infrared absorbance (1100−1850 cm^{-1}, std. ± 0.1−2%) for both GO-1 L (blue) and GO-3 L (red) indicates an *ca.* 110% increase instead of ~30% as a function of temperature. The normalization was performed by dividing to initial (prior to annealing) integrated absorbance values of 0.95 cm^{-1} for GO-1 L and 1.54 cm^{-1} for GO-3 L (1100−1850 cm^{-1}). Model structures are shown for processes involving (iii) only edge intrasheet interactions (GO-1 L), and (iv) both intrasheet and intersheet interactions (GO-3 L) for 60−125, 125−175, and 175−250 °C. Each species is identified with specific colors: epoxides (red), ethers (green), COOH (yellow), C═C (gray), C═O (pink), H for H_2O (aqua), O for H_2O, CO, and CO_2 (blue) using the ACD/ChemSketch Freeware, version 10.00, Advanced Chemistry Development, Inc., Toronto, ON, Canada, www.acdlabs.com, 2006.

S6a). The detection of CO_2 molecules indicates the formation of defects in the graphene basal plane. Such defects occur in the form of holes and have been predicted by MD simulations[36] and observed by high-resolution transmission electron microscopy.[37] The mechanism for void formation by CO_2 production is believed to be based on the reaction of dissociative oxygen (from the gas or water phase) with oxygen-functionalized basal plane sites and possibly epoxide migration to the edges.[38] It has also been proposed that carbon−carbon bonds below an epoxy group relax when aligned one dimensionally,[39] resulting in the introduction of cracks upon reduction.[40] Simultaneous decomposition of epoxides with carbonyl formation during annealing indicates that one source of basal plane defects is the epoxide removal (ring-opening), similar to the case of fullerenes *via* nucleophilic attack[41] but can also exist intrinsic upon oxidation.[42] In all proposed mechanisms, the presence of water molecules in close proximity to the reactants is essential for facilitating the reaction.

There are other mechanisms, such as edge interactions,[43] which can lead to quinone-like carbonyl[44] formation in both single and multilayered GO, as described in Supporting Information Figure S7. While these contribute to the process, they only contribute to a small fraction of the observed carbonyls.

To explain the large formation of these carbonyl species at ~175 °C, DFT calculations have been performed using a defective GO model with a localized etch hole,

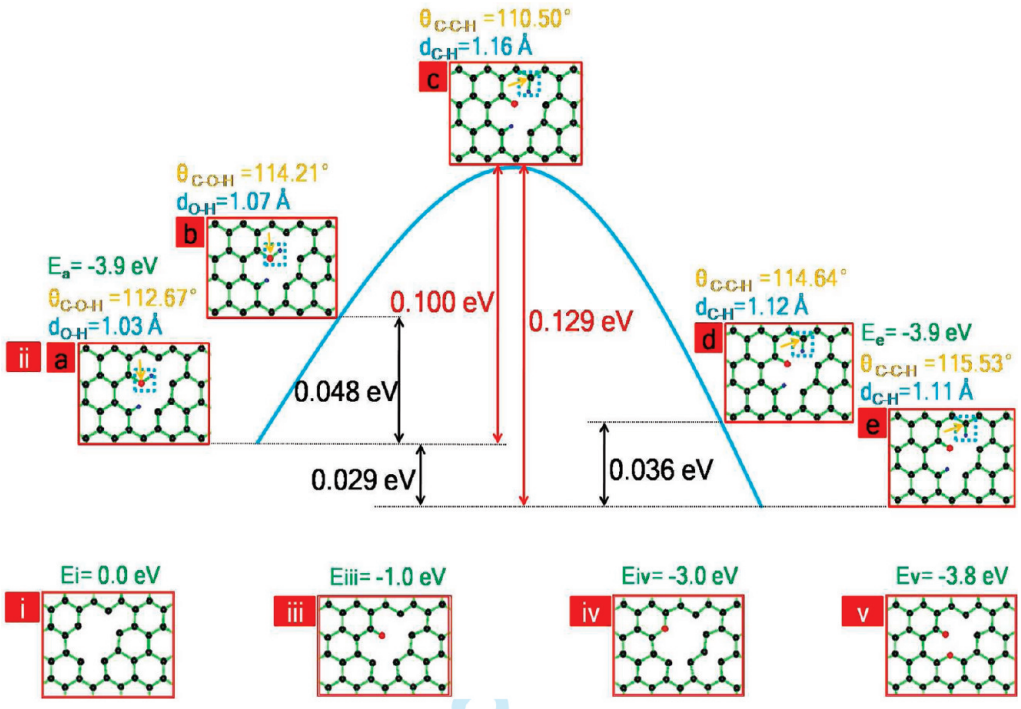

Figure 4. Activation energy calculations showing transformations between a hydroxyl and a carbonyl at an etch hole (i). (ii) The transition barriers for the transformation from structures a to e are shown for a total activation energy of 0.1 eV (forward direction) and 0.129 eV (reverse direction) (labeled in red). Structure a represents one H_2O reacting with the hole I forming a hydroxyl and a C−H bond (3.9 eV energy released-exothermic reaction). Structure e indicates one H_2O reacting with the hole I forming a carbonyl and two C−H bonds releasing 3.9 eV energy (exothermic reaction). Tilt angles (C−O−H for "a, b" and C−C−H for "d, e, f") in orange and the calculated bond lengths in blue are shown at each transformation stage on top of each structure. Energy calculations are shown in green for reactions between water molecules and etch holes with carbon dangling bonds. (iii) One H_2O reacts with (i) forming a carbonyl and H_2 (releases 1.0 eV energy, exothermic reaction). (iv) One H_2O reacts with (i) and forms an ether and H_2 (releases 3.0 eV energy, exothermic). (v) Two H_2Os react with (i) and forms a carbonyl, an ether group, and two H_2 molecules (releases 3.8 eV energy, exothermic reaction).

as illustrated in the lower left inset of Figure 4i. This model etch hole involves three carbon vacancies and is used to calculate how H_2O molecules can react with one or more dangling bonds, created *via* CO_2 production during the hole formation. The bottom of Figure 4 shows several possible reaction products with the formation energy associated with each reaction. One plausible path for carbonyl formation is an exothermic reaction lowering the energy of the system by 1.0 eV with a release of a H_2 shown in Figure 4iii that can happen when only one dangling bond exists. Another reaction path is through an exothermic reaction of a hydroxyl and C−H formation at two carbon dangling bonds which are formed reacting with a water molecule without a barrier and lower the energy by 3.9 eV as shown in Figure 4ii-a. Figure 4ii also shows a reaction process leading a carbonyl formation (Figure 4ii-e) with the same formation energy of 3.9 eV. This process has a small activation barrier (0.1 eV) and is likely to happen when more than one carbon dangling bond exist. The latter reaction path is the most likely route with the largest decrease in energy (3.9 eV), that is, leading to thermodynamically most stable products. These carbonyl groups subsequently react with residual epoxide groups which would migrate toward the etch hole, and such reactions will remove the carbonyl groups in the form of CO_2.[38] Small activation barriers (0.1 and 0.129 eV) in Figure 4ii-a−e also confirm that hydroxyls and carbonyls are easily reversible at the etch holes. The fact that OH and C═O formation energies are the same indicates that these reactions are reversible and consistent with the commonly known keto−enol tautomerism.[45] The incorporation of an oxygen in the basal plane through the C−O−C bond formation at two carbon dangling bond sites (resulting in cyclic ether formation along with a release of H_2) is also energetically favorable (Figure 4iv) with a formation energy of 3.0 eV. The reaction energy calculations also show that a cyclic ether and a carbonyl can form in an etch hole when two H_2O molecules react with two carbon dangling bonds releasing two H_2 (Figure 4v) and the formation energy (3.8 eV) is reduced from the sum (1.0 eV + 3.0 eV) due to the repulsive coulomb interaction between the oxygen atoms.

To verify the role of water chemistry and the mechanism of ketone and ester carbonyl formation in multilayered GO, we sought to displace the water by alcohol intercalation in the nanoscopically confined space between the GO sheets.[46] Intercalation of ethyl alcohol was achieved by immersion at room temperature for 4 days, as confirmed by an increase of interlayer spacing measured with XRD (Supporting Information, Figure

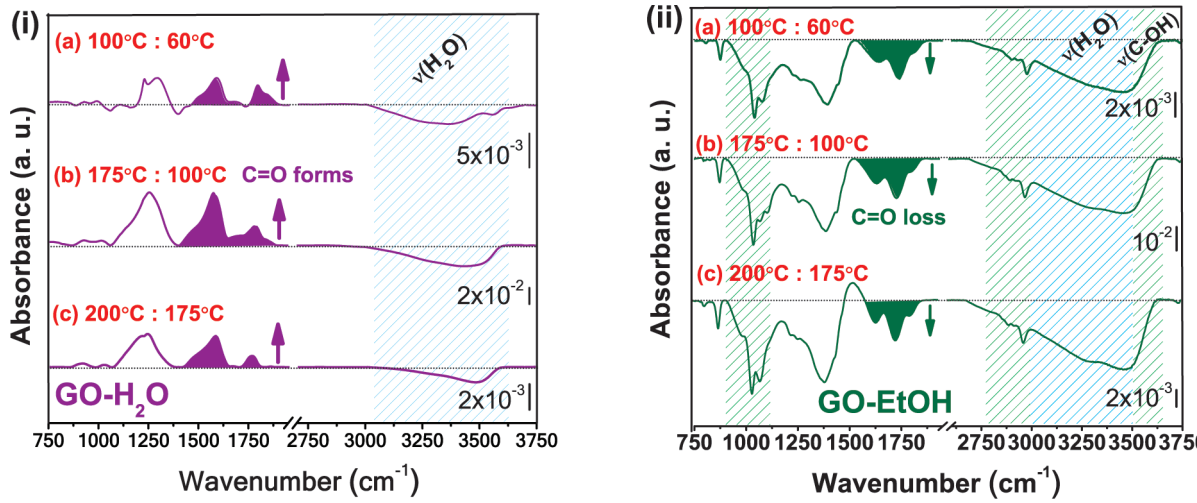

Figure 5. Comparison of water intercalated GO (GO-H_2O) and ethyl alcohol intercalated GO (GO-EtOH) for 4 days. Infrared differential spectra in transmission representing thermal reduction of (i) water intercalated GO (a−c) and (ii) ethyl alcohol intercalated GO films over the range of annealing temperatures: (a) 60−100, (b) 100−175, and (c) 175−200 °C. The stretching frequencies of C−OH and water are shown with blue dashed lines at (3000−3700 cm^{-1}) and C−OH and C−H vibrational frequencies of ethyl alcohol with green dashed lines.

S8). Spectroscopically, the IR data are consistent with the weakening of the H-bond network upon rearrangement (less total hydrogen bonding, Supporting Information Figure S9) as a result of H-bond distortion once ethyl alcohol is introduced.

The behavior upon annealing is best described by the differential IR spectra of multilayered GO containing water with and without ethyl alcohol shown in Figures 5i,ii. The enhancement in C═O formation upon annealing can be readily observed in the multilayered GO in the presence of water, while no carbonyl formation is observed with ethyl alcohol (Figure 5ii), as a result of water displacement by alcohol. The absence of carbonyl formation in alcohol-intercalated multilayered GO is attributed to the lower intercalated water concentration,[47] which minimizes the formation of etch holes and also the formation of carbonyls. The inactivity of intercalated alcohol upon annealing is shown in Supporting Information, Figure S9, where the integrated areas of OH stretch related modes do not change markedly over the 75−200 °C annealing range in sharp contrast to what is observed with water only (Figure 3i). The intercalation of alcohol therefore confirms the critical role played by water.

In summary, we have shown that intercalated water changes the entire interlayer chemistry in multilayered GO as compared with single layer GO. By using alcohol intercalation, we confirm that both defect (hole) formation and carbonyl formation is driven by intercalated water. First principles calculations further quantify the thermodynamic drive for carbonyl formation from water. The present work also suggests that multilayered GO is an interesting system to address issues related to water and other molecules in confined nanoscopic environments,[48] and should therefore stimulate further studies, such as 2D-IR Echo spectroscopy,[49] related to the role of confined molecules in carbon chemistry.

EXPERIMENTAL METHODS

Sample Preparation. GO was prepared using $NaNO_3$ and $KMnO_4$ in H_2SO_4 by the modified Hummers' method.[4] The GO thin films (1, 3, and 7 layers) were deposited from a suspension (0.18 mg/L) using amounts of 15, 45, and 105 mL and a vacuum-filtration method on a mixed cellulose ester membrane with 220 nm (Millipore). Further drying was performed for 12 h. Then the membrane was cut into sizes comparable to the substrate dimensions, slightly wetted with deionized water, and the upside was pressed against the substrate surface. The membrane with the GO film was allowed to dry and adhere to the substrate at room temperature under a 1 kg weight for 12 h. The weight was then removed and the membrane was dissolved using acetone without removing the GO films from the substrate. The samples were then immersed in pure acetone for 5 min at 60 °C. The samples were subsequently rinsed with methanol and dried with a nitrogen flow. The air-dried GO samples on each substrate were then characterized using Raman spectroscopy and AFM prior to annealing.[22]

The GO-ML samples were also prepared from a GO solution (0.18 mg/mL) taking in this case only 0.05 μL and drop casting this amount directly on clean SiO_2/Si substrates. Intercalation of multilayered GO was studied after drying the samples on the substrates in air. Each sample was soaked into 40 mL of ethyl alcohol (95%, 190 proof, 5 v/v % of water) in a centrifuge tube and kept closed. The ethyl alcohol solution was replaced with a fresh alcohol solution every day without disturbance of GO thin film. After blowing with nitrogen, each intercalated sample on the substrate was directly transferred into the annealing chamber in less than a minute within a laboratory humidity content of 34−40% (dew point of 8.0−11.0) and kept in vacuum during annealing in a closed system.

Analytical Characterization. All substrates (Si/SiO_2, fz-100, double-side polished) were cleaned mechanically using ethyl acetate, ethyl alcohol and distilled water (18 MΩ, Millipore) and then chemically in piranha solution [a mixture of H_2SO_4 and H_2O_2 (2:1, v/v)] by heating at 90 °C for 20 min to remove the organic residues from the surface. Each sample was transferred on these

clean surfaces either using membrane dissolution or direct drop-casting methods for thermal annealing.

Thermal annealing of GO samples on Si/SiO_2 substrates supported between tantalum-made clips was performed *in situ* (in vacuum) in an annealing chamber placed in an IR sample compartment with IR beam aligned at Brewster's angle of 70° for direct transmission. Therefore, no sample transfer was required between the spectrometer and the annealing chamber. Each temperature was monitored by a k-type thermocouple attached to the sample edge. The errors in each thermocouple reading calibrated using a pyrometer are systematic so that the relative measurements are accurate and reproducible. FTIR measurements for each specific temperature were performed at 60 °C within 5 min of annealing. The total annealing time per sample was ~18 h. The analysis of each sample was repeated twice to determine and quantify the reproducibility and consistency of the IR data.

UHV-XPS spectra were acquired in normal emission geometry using a conventional Mg X-ray source ($h\nu = 1253.6$ eV), pass energy at 20 eV, and with hemispherical electrostatic analyzer and a five channeltrons detector.

XRD diffraction of GO samples was recorded for two theta values from 2° to 40° in order to characterize the intersheet spacing. X-ray diffraction measurements were conducted with a Rigaku Ultima III diffractometer (Cu Kα radiation, X-ray wavelength of 1.54187A°, operating at 40 keV with a cathode current of 44 mA).

Theoretical Methods. The DFT calculations were performed using the Vienna *ab initio* simulation package (VASP),[50] where Kohn−Sham single-electron wave functions were expanded by a series of plane waves. The interactions between ions and valence electrons were described using the projected augmented wave (PAW)[51] method within local density approximation (LDA). The energy cutoff was chosen at 400 eV. In our model, three neighboring carbon atoms were removed in graphene's 4×4 unit cell to form a defect. Periodic boundary conditions were applied in the graphene plane, and a 12 Å vacuum region was added perpendicular to the graphene plane. The criterion for structural optimization was that total energy change between two ionic relaxation steps was smaller than 1 meV.

Acknowledgment. The authors acknowledge the financial support of the SWAN-NRI program and Texas Instruments (TI), technical expertise of J.-F. Veyan, and in-depth discussions with L. Colombo (TI) and with R. M. Wallace, E. Vogel, J. Kim, M. Kim, J-F. Veyan, and W. Kirk at UT Dallas. The authors declare that there are no competing financial interests. M.A. performed all IR spectroscopy work, including thermal annealing experiments and intercalation studies. C.M. prepared 1L, 3L and 7L GO thin films and obtained XPS spectra under M.C.'s supervision. C.G. and G.L. carried out all DFT simulations using theoretical methods. In discussing the main experimental results, K.C. proposed the critical role of water molecules confined between graphene layers and stimulated the subsequent modeling and additional experiments that validated this prediction. Y.J.C., M.C. and K.C. directed and supervised the experimental and theoretical research, respectively.

Supporting Information Available: Supportive FTIR, XPS, XRD data and corresponding simulated IR frequencies. This material is available free of charge *via* the Internet at http://pubs.acs.org.

REFERENCES AND NOTES

1. Park, S.; Ruoff, R. S. Chemical Methods for the Production of Graphenes. *Nat. Nanotechnol.* **2009**, *4*, 217–224.
2. Robinson, J. T. F.; Perkins, K.; Snow, E. S.; Wei, Z.; Sheehan, P. E. Reduced Graphene Oxide Molecular Sensors. *Nano Lett.* **2008**, *8*, 3137–3140.
3. Stoller, M. D.; Park, S.; Zhu, Y.; An, J.; Ruoff, R. S. Graphene-Based Ultracapacitors. *Nano Lett.* **2008**, *8*, 3498–3502.
4. Hummers, W. S.; Offeman, R. E. Preparation of Graphitic Oxide. *J. Am. Chem. Soc.* **1958**, *80*, 1339.
5. Staudenmaier, L. Verfahren zur Darstellung der Graphitsaure. *Ber. Deut. Chem. Ges.* **1898**, *31*, 1481–1499.
6. Brodie, B. C. On the Atomic Weight of Graphite. *Philos. Trans. R. Soc. London.* **1959**, *149*, 249–259.
7. Scholz, W.; Boehm, H. P. Untersuchungen am Graphitoxid. VI. Betrachtungen zur Struktur des Graphitoxids. *Anorg. Allg. Chem.* **1969**, *369*, 327–340.
8. Hirata, M.; Gotou, T.; Horiuchi, S.; Fujiwara, M.; Ohba, M. Thin-Film Particles of Graphite Oxide: High-Yield Synthesis and Flexibility of the Particles. *Carbon* **2004**, *42*, 2929–2937.
9. Stankovich, S.; Dikin, D. A.; Piner, R. D.; Kohlhaas, K. A.; Kleinhammes, A.; Jia, Y.; Wu, Y.; Nguyen, S. T.; Ruoff, R. S. Synthesis of Graphene-Based Nanosheets *via* Chemical Reduction of Exfoliated Graphite Oxide. *Carbon.* **2007**, *45*, 1558–1565.
10. Fan, X.; Peng, W.; Li, Y.; Li, X.; Wang, S.; Zhang, G.; Zhang, F. Deoxygenation of Exfoliated Graphite Oxide Under Alkaline Conditions: A Green Route to Graphene Preparation. *Adv. Mater.* **2008**, *20*, 4490–4493.
11. Szabó, T.; Berkesi, O.; Forgo, P.; Josepovits, K.; Sanakis, Y.; Petridis, D.; Dekany, I. Evolution of Surface Functional Groups in a Series of Progressively Oxidized Graphite Oxides. *Chem. Mater.* **2006**, *18*, 2740–2749.
12. Mattevi, C.; Eda, G.; Agnoli, S.; Miller, S.; Mkhoyan, K. A.; Celik, O.; Mastrogiovanni, D.; Granozzi, G.; Garfunkel, E.; Chhowalla, M. Evolution of Electrical, Chemical, and Structural Properties of Transparent and Conducting Chemically Derived Graphene Thin Films. *Adv. Funct. Mater.* **2009**, *19*, 2577–2583.
13. Eda, G.; Fanchini, G.; Chhowalla, M. Large-Area Ultrathin Films of Reduced Graphene Oxide as a Transparent and Flexible Electronic Material. *Nat. Nanotechnol.* **2008**, *3*, 270–274.
14. Tung, V. C.; Allen, M. J.; Yang, Y.; Kaner, R. B. High-Throughput Solution Processing of Large-Scale Graphene. *Nat. Nanotechnol.* **2009**, *4*, 25–29.
15. Becerril, H. A.; Mao, J.; Liu, Z.; Stoltenberg, R. M.; Bao, Z.; Chen, Y. Evaluation of Solution-Processed Reduced Graphene Oxide Films as Transparent Conductors. *ACS Nano* **2008**, *2*, 463–470.
16. Gao, X.; Jang, J.; Nagase, S. Hydrazine and Thermal Reduction of Graphene Oxide: Reaction Mechanisms, Product Structures, and Reaction Design. *J. Phys. Chem. C* **2010**, *114*, 832–842.
17. Jung, I.; Field, D. A.; Clark, N. J.; Zhu, Y.; Yang, D.; Piner, R. D.; Stankovich, S.; Dikin, D. A.; Geisler, H.; Ventrice, C. A., Jr.; *et al.* Reduction Kinetics of Graphene Oxide Determined by Electrical Transport Measurements and Temperature Programmed Desorption. *J. Phys. Chem. C* **2009**, *113*, 18480–18486.
18. Liang, M.; Luo, B.; Zhi, L. Application of Graphene and Graphene-Based Materials in Clean Energy-Related Devices. *Int. J. Energy Res.* **2009**, *33*, 1161–1170.
19. Wilson, N. R.; Pandey, P. A.; Beanland, R.; Young, R. J.; Kinloch, I. A.; Gong, L.; Liu, Z.; Suenaga, K.; Rourke, J. P.; York, S. J.; *et al.* Graphene Oxide: Structural Analysis and Application as a Highly Transparent Support for Electron Microscopy. *ACS Nano* **2009**, *3*, 2547–2556.
20. Park, S.; Lee, K.-S.; Bozoklu, G.; Cai, W.; Nguyen, S. B. T.; Ruoff, R. S. Graphene Oxide Papers Modified by Divalent Ions—Enhancing Mechanical Properties *via* Chemical Cross-Linking. *ACS Nano* **2008**, *2*, 572–578.
21. Stoller, M. D.; Park, S.; Zhu, Y.; An, J.; Ruoff, R. S. The Chemistry of Graphene Oxide. *Chem. Soc. Rev.* **2010**, *39*, 228–240.
22. Mkhoyan, K. A.; Contryman, A. W.; Silcox, J.; Stewart, D. A.; Eda, G.; Mattevi, C.; Miller, S.; Chhowalla, M. Atomic and Electronic Structure of Graphene-Oxide. *Nano Lett.* **2009**, *9*, 1058–1063.
23. Buchsteiner, A.; Lerf, A.; Pieper, J. Water Dynamics in Graphite Oxide Investigated with Neutron Scattering. *J. Phys. Chem. B.* **2006**, *110*, 22328–22338.
24. Yu, D.; Dai, L. Self-Assembled Graphene/Carbon Nanotube Hybrid Films for Supercapacitors. *J. Phys. Chem. Lett.* **2010**, *1*, 467–470.

25. Cassagneau, T.; Fendler, J. H. High Density Rechargeable Lithium-Ion Batteries Self-Assembled from Graphite Oxide Nanoplatelets and Polyelectrolytes. *Adv. Mater.* **1998**, *10*, 877–881.
26. Park, S.; An, J.; Suk, J. W.; Ruoff, R. S. Graphene-Based Actuators. *Small.* **2010**, *6*, 210–212.
27. Chen, C.; Rosenblatt, S.; Bolotin, K. I.; Kalb, W.; Kim, P.; Kymissis, I.; Stormer, H. L.; Heinz, T. F.; Hone, J. Performance of Monolayer Graphene Nanomechanical Resonators with Electrical Readout. *Nat. Nanotechnol.* **2009**, *4*, 861–867.
28. Bunch, J. S.; Van der Zande, A. M.; Verbridge, S. S.; Frank, I. W.; Tanenbaum, D. M.; Parpia, J. M.; Craighead, H. G.; McEuen, P. L. Electromechanical Resonators from Graphene Sheets. *Science* **2007**, *315*, 490–493.
29. Dikin, D. A.; Stankovich, S.; Zimney, E. J.; Piner, R. D.; Dommett, G. H. B.; Evmenenko, G.; Nguyen, S. T.; Ruoff, R. S. Preparation and Characterization of Graphene Oxide Paper. *Nature* **2007**, *448*, 457–460.
30. Kim, S. Y.; Park, H. S. The Importance of Edge Effects on the Intrinsic Loss Mechanisms of Graphene Nanoresonators. *Nano Lett.* **2009**, *9*, 969–974.
31. Wang, Y. Z.; Shi, Q.; Huang, Y.; Ma, Y. F.; Wang, C. Y.; Chen, M. M.; Chen, Y. S. Supercapacitor Devices Based on Graphene Materials. *J. Phys. Chem. C* **2009**, *113*, 13103–13107.
32. Medhekar, N. V.; Ramasubramaniam, A.; Ruoff, R. S.; Shenoy, V. B. Hydrogen Bond Networks in Graphene Oxide Composite Paper: Structure and Mechanical Properties. *ACS Nano* **2010**, *4*, 2300–2306.
33. Jeong, H.; Colakerol, L.; Jin, M. H.; Glans, P.; Smith, K. E.; Lee, Y. H. Unoccupied Electronic States in Graphite Oxides. *Chem. Phys. Lett.* **2008**, *460*, 499–502.
34. Lerf, A.; He, H.; Forster, M.; Klinowski, J. Structure of Graphite Oxide Revisited. *J. Phys. Chem. B* **1998**, *102*, 4477–4482.
35. Peckett, J.; Trens, W. P.; Gougeon, R. D.; Pöppl, A.; Harris, R. K.; Hudson, M. J. Electrochemically Oxidized Graphite. Characterization and Some Ion Exchange Properties. *Carbon* **2000**, *38*, 345–353.
36. Bagri, A.; Mattevi, C.; Acik, M.; Chabal, Y. J.; Chhowalla, M.; Shenoy, V. Structural Evolution During the Reduction of Chemically Derived Graphene Oxide. *Nat. Chem.* **2010**, *2*, 581–587.
37. Gümez-Navarro, C.; Meyer, J. C.; Sundaram, R. S.; Chuvilin, A.; Kurasch, S.; Burghard, M.; Kern, K.; Kaiser, U. Atomic Structure of Reduced Graphene Oxide. *Nano Lett.* **2010**, *10*, 1144–1148.
38. Radovic, L. R. Active Sites in Graphene and the Mechanism of CO_2 Formation in Carbon Oxidation. *J. Am. Chem. Soc.* **2009**, *131*, 17166–17175.
39. Li, J.-L.; Kudin, K. N.; McAllister, M. J.; Prud'Homme, R. K.; Aksay, I. A; Roberto, C. Oxygen-Driven Unzipping of Graphitic Materials. *Phys. Rev. Lett.* **2006**, *96*, 176101–176104.
40. Bourlinos, A. B.; Gournis, D.; Petridis, D.; Szabo, T.; Szeri, A.; Dekany, I. Graphite Oxide: Chemical Reduction to Graphite and Surface Modification with Primary Aliphatic Amines and Amino Acids. *Langmuir* **2003**, *19*, 6050–6055.
41. Taylor, R. Addition Reactions of Fullerenes. *C. R. Chim.* **2006**, *9*, 982–1000.
42. Xu, Z.; Xue, K. Engineering Graphene by Oxidation: A First-Principles Study. *Nanotechnology* **2010**, *21*, 045704−045710.
43. Boehm, H. P. Some Aspects of the Surface Chemistry of Carbon Blacks and Other Carbons. *Carbon* **1994**, *32*, 759–769.
44. Kundu, S.; Wang, Y.; Xia, W.; Muhler, M. Thermal Stability and Reducibility of Oxygen-Containing Functional Groups on Multiwalled Carbon Nanotube Surfaces: A Quantitative High-Resolution XPS and TPD/TPR Study. *J. Phys. Chem. C* **2008**, *112*, 16869–16878.
45. Peckett, J. W.; Trens, P.; Gougeon, R. D.; Pöppl, A.; Harris, R. K.; Hudson, M. J. Electrochemicaly Oxidized Graphite. Characterisation and Some Ion Exchange Properties. *Carbon* **2000**, *38*, 345–353.
46. Maréchal, Y. *The Hydrogen Bond and the Water Molecule*, 1st ed.; Elsevier: Italy, 2007.
47. Wagner, G. W; Chen, Q; Wu, Y. Reactions of VX, GD, and HD with Nanotubular Titania. *J. Phys. Chem. C* **2008**, *112*, 11901–11906.
48. Moilanen, D. E.; Spry, D. B.; Levinger, N. E.; Fayer, M. D. *J. Am. Chem. Soc.* **2007**, *129*, 14311–14318.
49. Asbury, J. B.; Steinel, T.; Fayer, M. D. Vibrational Echo Correlation Spectroscopy Probes of Hydrogen Bond Dynamics in Water and Methanol. *J. Lumin.* **2004**, *107*, 271–286.
50. Kresse, G.; Furthmüller, J. Efficiency of *ab-Initio* Total Energy Calculations for Metals and Semiconductors Using a Plane-Wave Basis Set. *J. Comput. Mater. Sci.* **1996**, *6*, 15–50.
51. Blöchl, P. E. Projector Augmented-Wave Method. *Phys. Rev. B.* **1994**, *50*, 17953–17979.